PROCEEDINGS OF SCIENCE

NNLO QCD calculations with CoLoRFulNNLO

Adam Kardos[*†]
Institute of Physics, University of Debrecen, H-4010 Debrecen, PBox 105, Hungary
E-mail: kardos.adam@science.unideb.hu

Gábor Somogyi
MTA-DE Particle Physics Research Group, University of Debrecen, 4010 Debrecen, PO Box 105, Hungary
E-mail: somogyi.gabor@science.unideb.hu

Zoltán Tulipánt
MTA-DE Particle Physics Research Group, University of Debrecen, 4010 Debrecen, PO Box 105, Hungary
E-mail: tulipant.zoltan@science.unideb.hu

The strong coupling is one fundamental parameter of the standard model. Its most precise determination is of fundamental importance. To contribute to the world average the calculation has to fit certain criteria. One of these is to have Next-to-Next-to-Leading Order accuracy in the fixed-order calculation. With the CoLoRFulNNLO subtraction method developed for electron-positron annihilation and new predictions become available at NNLO for observables such as the energy-energy correlation, we use this to extract the strong coupling using data measured by the OPAL and SLD detectors. To further enhance the region of validity of the predictions the fixed-order result was matched to already available resummed predictions.

13th International Symposium on Radiative Corrections (Applications of Quantum Field Theory to Phenomenology)
25-29 September, 2017
St. Gilgen, Austria

[*]Speaker.

[†]The research was supported by grant K 125105 of the National Research, Development and Innovation Office in Hungary and the Premium Postdoctoral Fellowship Programme of the Hungarian Academy of Sciences.

PoS(RADCOR2017)018

1. Introduction

The standard model of particle physics operates with several parameters. Among these we can find the strong coupling which is usually given at a scale corresponding to the mass of the Z boson. The value of α_S appears as a world average [1] composed of several measurements carried out at various experiments. Among these measurements a large number was performed in electron-positron annihilation using observables like the three-jet rate or the six standard event shape variables (thrust, C-parameter, jet broadenings, heavy jet mass and the two-to-three jet transition variable) [2, 3, 4, 5, 6].

The extraction of α_S using data from high-energy experiments relies upon fitting theoretical predictions to measurement data. Since fixed-order predictions are made at the parton level and detectors observe hadrons parton-level predictions have to be supplemented with a hadronization model or the hadron-level data has to be unfolded to the parton level to have a meaningful comparison. The theoretical prediction is treated as a function of α_S and the strong coupling is considered as a fitting parameter looking for the best fit to data.

In order to contribute to the world average the fixed-order prediction has to have at least Next-to-Next-to Leading Order (NNLO) accuracy in QCD. For a large class of observables there are regions in phase space where perturbation theory breaks down due to large logarithmic contributions necessitating the explicit summation of contributions coming from all orders. With the matching of resummed and fixed-order predictions the region of validity of the prediction can be extended.

The CoLoRFulNNLO subtraction scheme [7, 8, 10] made it possible to compute the NNLO QCD correction to three further event shape observables in electron-positron annihilation: oblateness, energy-energy correlation (EEC) [9] and jet cone energy fraction [10]. For EEC Next-to-Next-to Leading Logarithmic (NNLL) resummation is available [11] in the back-to-back region thus matching the NNLO with the NNLL resummed predictions makes a perfect candidate for an observable which can be used to extract the strong coupling since this observable was widely measured in several experiments. In this talk we discuss how in a recent publication [12] the CoLoRFulNNLO subtraction method and NNLL resummation were enrolled to obtain the value of $\alpha_S(m_Z)$ using OPAL [13] and SLD [14] data. A further motivation behind choosing EEC as an observable is that in electron-positron annihilation only global event shape observables and jet rates were used so far for this purpose while EEC is based on two-particle correlations.

We would like to conclude this section mentioning that there is a growing interest in EEC nowadays. There is an attempt to obtain the NLO QCD correction to EEC in a fully analytic way using very recent, state-of-the-art techniques derived in multiloop calculations [15].

2. Definition and fixed order

Energy-energy correlation was defined almost 40 years ago [16] in order to quantify two-particle correlations in electron-positron collisions:

$$\frac{1}{\sigma_t}\frac{d\Sigma(\chi)}{d\cos\chi} \equiv \frac{1}{\sigma_t}\int \sum_{i,j} \frac{E_i E_j}{Q^2} d\sigma_{e^+e^-\to ij+X}\,\delta(\cos\chi + \cos\theta_{ij})\,, \tag{2.1}$$

where σ_t is the total cross section corresponding to $e^+e^- \to$ hadrons, Q is the CM energy of the collision, $\cos\theta_{ij}$ is the enclosed angle between two hadrons observed and the double sum runs over all possible pairs of final state hadrons produced in the event. The back-to-back region corresponds to the region of $\chi \to 0$.

EEC is calculated in QCD perturbation theory as a series expansion in α_S taking the following form up to the NNLO contribution:

$$\left[\frac{1}{\sigma_t}\frac{d\Sigma(\chi,\mu)}{d\cos\chi}\right]_{f.o.} = \frac{\alpha_S(\mu)}{2\pi}\frac{d\bar{A}(\chi,\mu)}{d\cos\chi} + \left(\frac{\alpha_S(\mu)}{2\pi}\right)^2\frac{d\bar{B}(\chi,\mu)}{d\cos\chi} + \left(\frac{\alpha_S(\mu)}{2\pi}\right)^3\frac{d\bar{C}(\chi,\mu)}{d\cos\chi} + \mathcal{O}(\alpha_S^4), \tag{2.2}$$

where $\bar{A}$, $\bar{B}$ and $\bar{C}$ stand for the LO, NLO and NNLO contributions, respectively. The bar over different contributions emphasizes that the total cross section was used for normalization.

To calculate the first three terms in the perturbative expansion we used the CoLoRFulNNLO subtraction method as it is implemented in the numerical code called `MCCSM` (Monte Carlo for the CoLoRFulNNLO Subtraction Method). To get a glimpse of the inner workings of the subtraction method let us consider a completely general jet measurement function J which is IR-safe. For this physical observable the cross section, as a perturbative series in terms of α_S, takes the form of

$$\sigma[J] = \sigma^{LO}[J] + \sigma^{NLO}[J] + \sigma^{NNLO}[J] + \dots, \tag{2.3}$$

here $\sigma^{LO}[J]$, $\sigma^{NLO}[J]$ and $\sigma^{NNLO}[J]$ stand for the LO, NLO and NNLO contributions, respectively. The LO term is the easiest to calculate since it is always finite due to phase space cuts:

$$\sigma^{LO}[J] = \int_m d\sigma_m^B J_m, \tag{2.4}$$

where $d\sigma^B$ contains the Born squared matrix element and the integration is performed over an m-parton phase space if our process has m final state partons at Born level. The NLO term is composed of two separate contributions and can be written as

$$\sigma^{NLO}[J] = \sigma_{m+1}^{NLO}[J] + \sigma_m^{NLO}[J] = \int_{m+1} d\sigma_{m+1}^R J_{m+1} + \int_m d\sigma_m^V J_m, \tag{2.5}$$

where the first term corresponds to the case where there is one more massless parton in the final state, hence dubbed the real-emission part, while the other contains a virtual exchange of a massless parton, commonly known as the virtual part. While the first contribution is divergent due to kinematic singularities appearing in the phase space the second one contains explicit ε poles coming from the loop integral. When the phase space integral over $m+1$ parton is carried out in $d = 4-2\varepsilon$ dimensions the appearing poles exactly cancel those coming from the second term resulting in a finite correction for IR-safe observables due to the KLN theorem. To avoid the analytical integration in d dimensions in the first term subtractions can be introduced mimicking the singularity structure of the real-emission matrix element making the first integral finite even in 4 dimensions. Of course to reinstate physicality the subtractions have to be added back in an integrated form:

$$\int_{m+1}\left[d\sigma_{m+1}^R J_{m+1} - d\sigma_{m+1}^{R,A_1} J_m\right]_{d=4} + \int_m \left[d\sigma_m^V J_m + \int_1 d\sigma_{m+1}^{R,A_1} J_m\right]_{d=4}. \tag{2.6}$$

The NNLO contribution can be disentangled into three terms having completely different nature, namely:

$$\sigma^{\mathrm{NNLO}}[J] = \sigma^{\mathrm{NNLO}}_{m+2}[J] + \sigma^{\mathrm{NNLO}}_{m+1}[J] + \sigma^{\mathrm{NNLO}}_{m}[J] = \int_{m+2} \mathrm{d}\sigma^{\mathrm{RR}}_{m+2} J_{m+2} + \int_{m+1} \mathrm{d}\sigma^{\mathrm{RV}}_{m+1} J_{m+1} + \int_{m} \mathrm{d}\sigma^{\mathrm{VV}}_{m} J_{m}\,. \tag{2.7}$$

The first term is the $m+2$-parton (double-real, RR) contribution containing matrix elements responsible for the emission of two additional massless partons, the $m+1$-parton (real-virtual, RV) contribution has kinematic singularities due to the emission of one extra parton and explicit ε poles due to the virtual exchange of one massless parton, finally the m-parton (double-virtual, VV) contribution only contains explicit ε poles due to the virtual exchange of two massless partons. As in the case of NLO, subtractions are introduced to regularize singularities of kinematic origin associated to unresolved extra parton emission(s).

For the $m+2$-parton contribution subtractions have to be introduced to regularize the singly- (A_1) and doubly-unresolved emissions (A_2). Since the presence of subtractions is not limited to around their respective limits even the subtractions can develop spurious singularities away from their singularity region. To remove these spurious singularities an additional term has to be included (A_{12}). After the inclusion of all the terms the $m+2$-parton line becomes finite in $d=4$ dimensions:

$$\sigma^{\mathrm{NNLO}}_{m+2} = \int_{m+2} \left\{ \mathrm{d}\sigma^{\mathrm{RR}}_{m+2} J_{m+2} - \mathrm{d}\sigma^{\mathrm{RR,A_2}}_{m+2} J_m - \left[\mathrm{d}\sigma^{\mathrm{RR,A_1}}_{m+2} J_{m+1} - \mathrm{d}\sigma^{\mathrm{RR,A_{12}}}_{m+2} J_m \right] \right\}_{d=4}. \tag{2.8}$$

In the $m+1$-parton line alongside from the real-virtual contribution the integrated version of the A_1 subtractions defined for the $m+2$-parton line appear also, hence subtractions are introduced not only to regularize the kinematic singularities coming from the real-virtual part but also from the integrated A_1 terms. When all necessary subtractions are incorporated the $m+1$-parton line becomes finite in $d=4$ dimensions:

$$\sigma^{\mathrm{NNLO}}_{m+1} = \int_{m+1} \left\{ \left(\mathrm{d}\sigma^{\mathrm{RV}}_{m+1} + \int_1 \mathrm{d}\sigma^{\mathrm{RR,A_1}}_{m+2} \right) J_{m+1} - \left[\mathrm{d}\sigma^{\mathrm{RV,A_1}}_{m+1} + \left(\int_1 \mathrm{d}\sigma^{\mathrm{RR,A_1}}_{m+2} \right)^{\mathrm{A_1}} \right] J_m \right\}_{d=4}, \tag{2.9}$$

Finally, the m-parton line does not contain any kinematic singularity but instead explicit ε poles coming from the double-virtual contribution. These poles are cancelled by the remaining integrated subtraction terms resulting in a finite m-parton contribution:

$$\sigma^{\mathrm{NNLO}}_{m} = \int_{m} \left\{ \mathrm{d}\sigma^{\mathrm{VV}}_{m} + \int_2 \left[\mathrm{d}\sigma^{\mathrm{RR,A_2}}_{m+2} - \sigma^{\mathrm{RR,A_{12}}}_{m+2} \right] + \int_1 \left[\mathrm{d}\sigma^{\mathrm{RV,A_1}}_{m+1} + \left(\int_1 \mathrm{d}\sigma^{\mathrm{RR,A_1}}_{m+2} \right)^{\mathrm{A_1}} \right] \right\}_{d=4} J_m\,. \tag{2.10}$$

Our theoretical predictions obtained with the help of `MCCSM` for EEC is shown in Fig. (1). The non-overlapping of the NLO and NNLO uncertainty bands indicates that the scale uncertainties are underestimated with the conventional sweep between $\mu = Q/2$ and $2Q$. The large difference between NNLO prediction and measurement indicates that power corrections are sizable, thus for a meaningful comparison to experimental data hadronization effects must be taken into account or data has to be unfolded to the parton level.

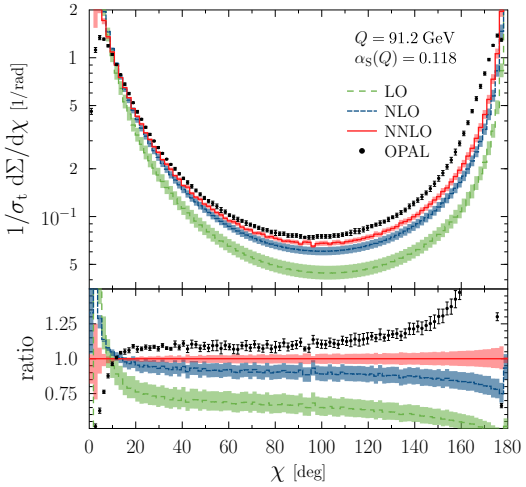

Figure 1: Fixed order predictions for EEC in the first three orders of QCD perturbation theory and data measured by the OPAL collaboration [13]. On the lower panel ratios are shown with respect to the NNLO prediction. The bands represent the uncertainty from scale variation obtained by varying μ between $Q/2$ and $2Q$.

3. Resummed predictions

The most precise resummation for EEC in the back-to-back region is available at NNLL [11]. Formally the resummed prediction can be written as

$$\left[\frac{1}{\sigma_t}\frac{d\Sigma(\chi,\mu)}{d\cos\chi}\right]_{\text{res.}} = \frac{Q^2}{8}H(\alpha_S(\mu))\int_0^\infty db\, b J_0(bQ\sqrt{y})S(Q,b)\,, \tag{3.1}$$

where $y = \sin^2\chi/2$ and $S(Q,b)$ is the Sudakov form factor defined on impact parameter space:

$$S(Q,b) = \exp\left\{-\int_{b_0^2/b^2}^{Q^2}\frac{dq^2}{q^2}\left[A(\alpha_S(q^2))\log\frac{Q^2}{q^2} + B(\alpha_S(q^2))\right]\right\}, \tag{3.2}$$

where $A(\alpha_S)$, $B(\alpha_S)$ and $H(\alpha_S)$–the hard function–are defined in QCD perturbation theory and are free of logarithmic terms:

$$A(\alpha_S) = \sum_{n=1}^{\infty}\left(\frac{\alpha_S}{4\pi}\right)^n A^{(n)}, \quad B(\alpha_S) = \sum_{n=1}^{\infty}\left(\frac{\alpha_S}{4\pi}\right)^n B^{(n)}, \quad H(\alpha_S) = 1 + \sum_{n=1}^{\infty}\left(\frac{\alpha_S}{4\pi}\right)^n H^{(n)}. \tag{3.3}$$

In principle[1] to retain NNLL accuracy we need $A^{(1)}, A^{(2)}, A^{(3)}, B^{(1)}, B^{(2)}, H^{(1)}$ and $H^{(2)}$.

The resummed predictions at various orders with their respective scale uncertainties and OPAL measurement as a reference are depicted on Fig. (2). The resummed predictions, in particular the NNLL, successfully reproduce the Sudakov shoulder at small angles as seen in the measurement. Going to higher angles, the measurement and predictions start to deviate, hence the resummed prediction by itself cannot describe the measurement. This necessitates the matching of fixed-order and resummed predictions in order to obtain a theoretical prediction over a wide range of angles.

[1] As we will see we will not need the hard function explicitly by virtue of the matching scheme we employ.

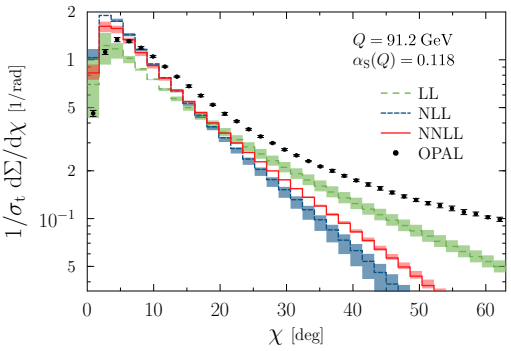

Figure 2: Resummed predictions at various logarithmic orders with their respective scale uncertainty bands obtained by varying μ between $Q/2$ and $2Q$. Data obtained by the OPAL collaboration is also shown.

4. The matching procedure

The resummed prediction contains specific logarithms from each order of perturbation theory which are summed up hence appearing in an exponentiated form. A subset of these logs can also be found in the fixed order prediction hence the most naive matching: adding up the resummed and fixed-order predictions cannot result in a physical result due to double counting of those logs.

In order to avoid double counting those logs have to be subtracted from the sum of the resummed and fixed-order predictions. This can be achieved by expanding the resummed result in α_S and subtracting terms from the sum which appear in the same or lower order of α_S as our fixed-order prediction:

$$\frac{1}{\sigma_t}\frac{d\Sigma(\chi,\mu)}{d\cos\chi} = \left[\frac{1}{\sigma_t}\frac{d\Sigma(\chi,\mu)}{d\cos\chi}\right]_{\text{res.}} + \left[\frac{1}{\sigma_t}\frac{d\Sigma(\chi,\mu)}{d\cos\chi}\right]_{\text{f.o.}} - \left\{\left[\frac{1}{\sigma_t}\frac{d\Sigma(\chi,\mu)}{d\cos\chi}\right]_{\text{res.}}\right\}\Bigg|_{\text{f.o.}}. \tag{4.1}$$

This matching is called the naive R-matching scheme and it relies on the assumption that the resummed prediction is accurate enough to remove all the logs from the fixed-order prediction when expanded in terms of α_S. At NNLL+NNLO the remaining subleading logs in the fixed-order result drive the matched prediction to non-physical values well, inside the range which can be experimentally measured. In the absence of resummed predictions with higher accuracy the problem can be circumvented by applying the log-R matching scheme.

In order to perform the matching in the log-R scheme a cumulative observable has to be defined:

$$R(y,\mu) = \frac{1}{\sigma_t}\int_0^y dy' \frac{d\sigma(y',\mu)}{dy'}, \tag{4.2}$$

and the differential cross section in the original observable can be obtained by differentiating with respect to y. Also note that $R(y_{\max},\mu) = 1$, where $y_{\max}$ is the kinematically allowed maximal value of y. The perturbative expansion of the cumulative observable is:

$$[R(y,\mu)]_{\text{f.o.}} = 1 + \frac{\alpha_S(\mu)}{2\pi}\bar{\mathscr{A}}(y,\mu) + \left(\frac{\alpha_S(\mu)}{2\pi}\right)^2 \bar{\mathscr{B}}(y,\mu) + \left(\frac{\alpha_S(\mu)}{2\pi}\right)^3 \bar{\mathscr{C}}(y,\mu) + \mathscr{O}(\alpha_S^4). \tag{4.3}$$

On the other hand the resummed formula for R can be written as:

$$[R(y,\mu)]_{\text{res.}} = \left(1 + C_1\alpha_S + C_2\alpha_S^2 + \dots\right) \exp\left[Lg_1(\alpha_S L) + g_2(\alpha_S L) + \alpha_S g_3(\alpha_S L) + \dots\right] + \mathscr{O}(\alpha_S y)\,, \tag{4.4}$$

where $\mathscr{O}(\alpha_S y)$ stands for those terms which are not log enhanced. The g_n functions take the form:

$$g_n(\alpha_S L) = \sum_{i=1}^{\infty} G_{i,i+2-n} \left(\frac{\alpha_S}{2\pi}\right)^i L^{i+2-n} \tag{4.5}$$

where $L = \log y$. Taking the logarithm of the fixed-order result and expanding in α_S we get

$$\begin{aligned}\log[R(y,\mu)]_{\text{f.o.}} = {} & \frac{\alpha_S(\mu)}{2\pi}\bar{\mathscr{A}}(y,\mu) + \left(\frac{\alpha_S(\mu)}{2\pi}\right)^2 \left[\bar{\mathscr{B}}(y,\mu) - \frac{1}{2}\bar{\mathscr{A}}^2(y,\mu)\right] \\ & + \left(\frac{\alpha_S(\mu)}{2\pi}\right)^3 \left[\bar{\mathscr{C}}(y,\mu) - \bar{\mathscr{A}}(y,\mu)\bar{\mathscr{B}}(y,\mu) + \frac{1}{3}\bar{\mathscr{A}}^3(y,\mu)\right] + \mathscr{O}(\alpha_S^4)\,,\end{aligned} \tag{4.6}$$

similarly for the resummed expression:

$$\begin{aligned}\log[R(y,\mu)]_{\text{res.}} = {} & Lg_1(\alpha_S L) + g_2(\alpha_S L) + \alpha_S g_3(\alpha_S L) \\ & + \alpha_S C_1 + \alpha_S^2\left(C_2 - \frac{1}{2}C_1^2\right) + \alpha_S^3\left(C_3 - C_1C_2 + \frac{1}{3}C_1^3\right) + \mathscr{O}(\alpha_S^4)\,.\end{aligned} \tag{4.7}$$

We can arrive at the log-R matching scheme formula for NNLL+NNLO if the first three terms in the second line of Eq. (4.7) get replaced by those coming from the fixed order formula (Eq. (4.6)):

$$\begin{aligned}\log R(y,\mu) = {} & Lg_1(\alpha_S L) + g_2(\alpha_S L) + \alpha_S g_3(\alpha_S L) \\ & + \frac{\alpha_S(\mu)}{2\pi}\left[\bar{\mathscr{A}}(y,\mu) - G_{11}L - G_{12}L^2\right] \\ & + \left(\frac{\alpha_S(\mu)}{2\pi}\right)^2 \left[\bar{\mathscr{B}}(y,\mu) - \frac{1}{2}\bar{\mathscr{A}}^2(y,\mu) - G_{21}L - G_{22}L^2 - G_{23}L^3\right] \\ & + \left(\frac{\alpha_S(\mu)}{2\pi}\right)^3 \left[\bar{\mathscr{C}}(y,\mu) - \bar{\mathscr{A}}(y,\mu)\bar{\mathscr{B}}(y,\mu) + \frac{1}{3}\bar{\mathscr{A}}^3(y,\mu) - G_{32}L^2 - G_{33}L^3 - G_{34}L^4\right] \\ & + \mathscr{O}(\alpha_S^4)\,.\end{aligned} \tag{4.8}$$

By exponentiating the previous expression and differentiating it with respect to y we arrive at the log-R matching formula for our original observable.

By taking a look at Fig. (1) it becomes apparent that the fixed-order prediction for EEC not only diverges for small but also for large angles which in principle necessitates yet another resummation for the $y \to 1$ region to have a physical prediction even there. Provided having NNLO fixed-order predictions and NNLL resummation formula for $y \to 0$ it mandates for the use of log-R matching[2]. Because of the double divergent nature of the fixed-order EEC distribution the original definition

[2]This is not the only possibility: the coefficients of missing logarithms from the resummed expression could be obtained by a fitting procedure using the deep limit of the fixed-order calculation. This option is dropped since the calculation, though possible, very challenging at NNLO.

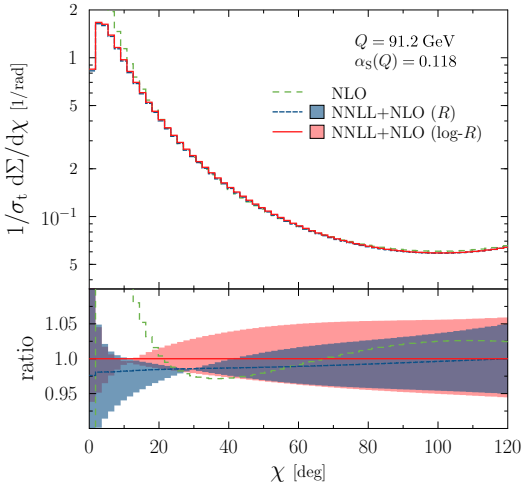

Figure 3: The NLO (green dashed) and NNLL+NLO matched predictions in the log-R (red) and R (blue dashed) schemes. The lower panel shows the ratio to the NNLL+NLO prediction using log-R matching while the bands correspond to the usual scale variation between $Q/2$ and $2Q$.

for the cumulative observable (Eq. (4.2)) cannot be used, instead we need one which suppresses the divergence appearing at large angles. One possible choice is:

$$\frac{1}{\sigma_t}\widetilde{\Sigma}(\chi,\mu) \equiv \frac{1}{\sigma_t}\int_0^{\chi} d\chi'(1+\cos\chi')\frac{d\Sigma(\chi',\mu)}{d\chi'}. \tag{4.9}$$

This modified version of the cumulative observable also fulfills the requirement that $\widetilde{\Sigma}(\chi_{\max},\mu)/\sigma_t = 1$, where $\chi_{\max} = 180^\circ$ and the original observable can be obtained by means of simple operations from $\widetilde{\Sigma}$:

$$\frac{1}{\sigma_t}\frac{d\Sigma(\chi,\mu)}{d\chi} = \frac{1}{1+\cos\chi}\frac{d}{d\chi}\left[\frac{1}{\sigma_t}\widetilde{\Sigma}(\chi,\mu)\right]. \tag{4.10}$$

In order to validate our log-R matched results we performed both the naive R and the log-R matching at NNLL+NLO. At this order the resummation is accurate enough to cancel all the logs from fixed order, and the predictions are depicted on Fig. (3). As it can be seen, both matched predictions provide the same result within scale uncertainties and the difference between the two schemes becomes very small at large angles.

5. Phenomenology

Our phenomenological studies are performed at $Q = 91.2\,\text{GeV}$ energy. As for the strong coupling we used $\alpha_S(Q) = 0.118$ and two- and three-loop running to obtain scale uncertainty bands at NLO and NNLO, respectively. On the left hand side of Fig. (4) a comparison is shown between NNLO and NNLL+NNLO. As it can be seen the fixed-order is ill-behaved as $\chi \to 0$ while the matched prediction remains physical in the whole range showing a nice Sudakov shoulder around

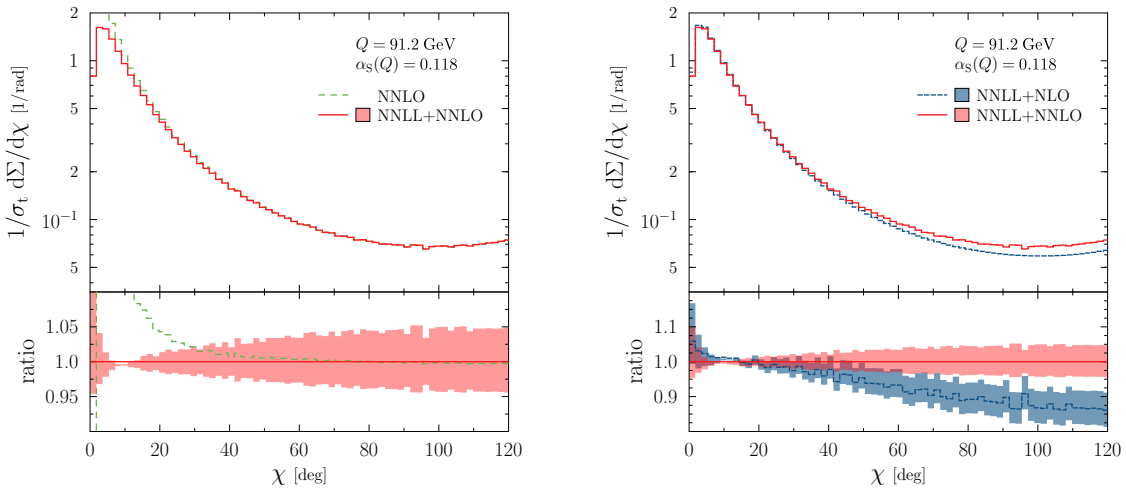

Figure 4: The left hand side shows the comparison between fixed-order and fixed-order matched with resummation. On the right hand side we compare our two matched results using NNLL resummation and NLO and NNLO for fixed-order, respectively. On the lower panels ratios are shown with respect to the NNLL+NNLO prediction. The bands, as usual, stand for scale uncertainty obtained by variation in the range of $[Q/2, 2Q]$.

Fit range	NNLL + NLO (R)		NNLL + NLO (log-R)		NNLL + NNLO (log-R)	
	$\alpha_S(m_Z)$	χ^2/d.o.f.	$\alpha_S(m_Z)$	χ^2/d.o.f.	$\alpha_S(m_Z)$	χ^2/d.o.f.
$0° < \chi < 63°$	0.133 ± 0.001	1.96	0.131 ± 0.003	1.21	0.129 ± 0.003	4.13
$15° < \chi < 63°$	0.132 ± 0.001	0.59	0.131 ± 0.003	0.54	0.128 ± 0.003	1.58
$15° < \chi < 120°$	0.135 ± 0.002	3.96	0.134 ± 0.004	5.12	0.127 ± 0.003	1.12

Table 1: Strong coupling values obtained at an energy scale corresponding to the mass of the Z boson with various fitting ranges but without hadronization effects incorporated.

5°. On the right hand side of Fig. (4) our two matched results are compared: using NNLL accuracy in the resummed part the matching was performed with NLO and NNLO. From the lower panel it is apparent that while the Sudakov shoulder remains almost the same at moderate to high angles the shape of the distribution changes significantly when going from NLO to NNLO.

Although as it was shown on Fig. (1) the hadronization corrections seem to be large an attempt can be made to extract α_S from our NNLL+NLO and NNLL+NNLO predictions using OPAL and SLD data without taking into account any of these effects. In order to obtain a value for α_S a range of the physical observable has to be defined on which the fitting procedure can be performed. In order to perform a fair comparison with the original NNLL+NLO computation we adopted the fit ranges already used in Ref. [11]. The resulting α_S values for the various ranges and theoretical predictions are tabulated in Tab. (1). By taking a look at the obtained α_S values it is clear that the neglected hadronization effects do have a significant contribution since all the α_S values are much larger than the world average, a clear indication of omitting a significant contribution. Judging by the goodness of fit the best value was obtained when the Sudakov shoulder region was

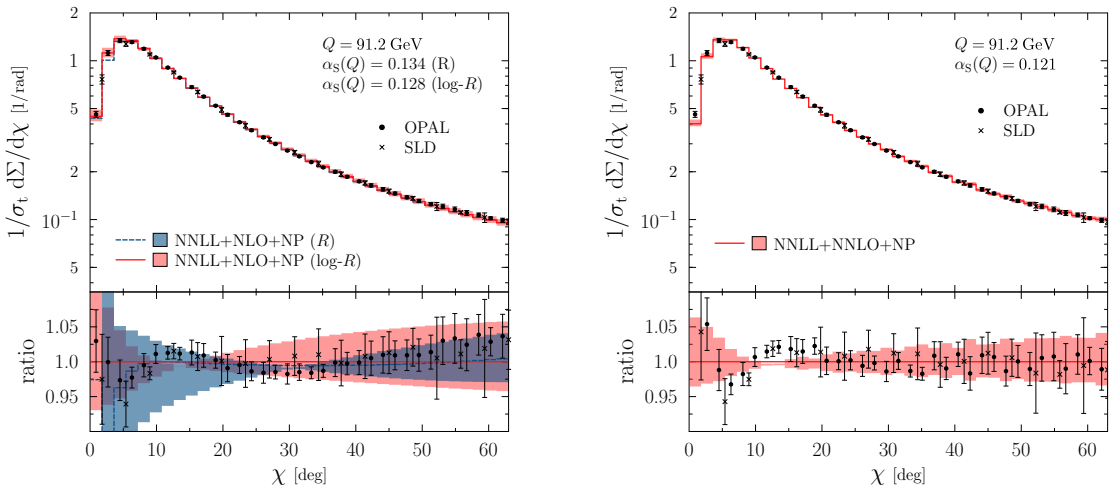

Figure 5: Our best α_S fits using various fixed-order predictions and matching schemes. The lower panels show the ratios compared to the predictions obtained with the log-R matching scheme. Bands correspond to scale variation in the range of $[Q/2, 2Q]$.

Accuracy	$\alpha_S(m_Z)$	a_1 [GeV^2]	a_2 [GeV]	χ^2/d.o.f.
NNLL+NLO(R)	$0.134^{+0.001}_{-0.009}$	$1.55^{+4.26}_{-1.54}$	$-0.13^{+0.50}_{-0.05}$	0.81
NNLL+NLO(log-R)	$0.128^{+0.002}_{-0.006}$	$1.17^{+1.46}_{-0.29}$	$0.13^{+0.14}_{-0.09}$	0.85
NNLL+NNLO(log-R)	$0.121^{+0.001}_{-0.003}$	$2.47^{+0.48}_{-2.38}$	$0.31^{+0.27}_{-0.05}$	1.18

Table 2: Result of our three-parameter fits involving the strong coupling and the two free parameters of the analytical hadronization model.

excluded from the fit range and the range was large enough to involve data from regions with larger angles and when the NNLL resummation was matched with our NNLO fixed-order prediction. By investigating the different results we conclude that the hadronization effects indeed play an important role and they also have a significant impact in the peak region.

There are two ways to incorporate hadronization effects: by using an analytic model or taking a fixed-order calculation, preferably a NLO computation, and matching it to a Shower Monte Carlo (SMC) program which contains a phenomenological model for hadronization. By comparing the fixed-order and hadron level predictions with the SMC we can obtain a bin-by-bin correction factor, applying this differential factor on our parton level predictions these can be brought to the hadron level. Since several SMC programs are available with their distinct hadronization models α_S extraction using this method needs a dedicated, detailed study which we leave for a future work and we use the former approach. In particular we chose the analytic hadronization model of Ref. [17] which was also used in Ref. [11].

In the hadronization model of Ref. [17] the Sudakov form factor is multiplied by

$$S_{\mathrm{NP}} = \mathrm{e}^{-\frac{1}{2}a_1 b^2}\,(1 - 2a_2 b)\,, \tag{5.1}$$

where b is the usual impact parameter while a_1 and a_2 are free model parameters. Thus when α_S is determined the one-parameter fit becomes a three-parameter fit involving a_1 and a_2 beside α_S. Our best fits to OPAL and SLD data are depicted on Fig. (5) and the obtained α_S and free parameter values with their respective χ^2/d.o.f. are tabulated on Tab. (2). Taking a look at the left hand side (NNLL+NLO) of Fig. (5) a clear trend is visible between data and fitted results. This slope disappears if NNLO corrections are taken into account thus the inclusion of such corrections is essential for the precision extraction of the strong coupling.

6. Conclusions

In this talk we have presented the first calculation of energy-energy correlation in electron-positron annihilation using NNLL resummation matched with an NNLO QCD fixed-order computation. Using an analytical hadronization model we were able to extract the value of α_S at the Z peak using OPAL and SLD data and found complete agreement with the world average within uncertainties. We observe that the inclusion of NNLO corrections is essential to get a shape compatible with the one observed by the experiments. A more detailed study is underway where hadronization corrections are obtained from SMC programs matched with NLO QCD calculations.

References

[1] S. Bethke, Nucl. Part. Phys. Proc. **282-284** (2017) 149.

[2] G. Dissertori, A. Gehrmann-De Ridder, T. Gehrmann, E. W. N. Glover, G. Heinrich and H. Stenzel, JHEP **0802** (2008) 040

[3] T. Becher and M. D. Schwartz, JHEP **0807** (2008) 034

[4] G. Dissertori, A. Gehrmann-De Ridder, T. Gehrmann, E. W. N. Glover, G. Heinrich, G. Luisoni and H. Stenzel, JHEP **0908** (2009) 036

[5] Y. T. Chien and M. D. Schwartz, JHEP **1008** (2010) 058

[6] R. Abbate, M. Fickinger, A. H. Hoang, V. Mateu and I. W. Stewart, Phys. Rev. D **83** (2011) 074021

[7] G. Somogyi, Z. Trócsányi and V. Del Duca, JHEP **0701** (2007) 070

[8] G. Somogyi and Z. Trócsányi, JHEP **0701** (2007) 052

[9] V. Del Duca, C. Duhr, A. Kardos, G. Somogyi and Z. Trócsányi, Phys. Rev. Lett. **117** (2016) no.15, 152004

[10] V. Del Duca, C. Duhr, A. Kardos, G. Somogyi, Z. Szőr, Z. Trócsányi and Z. Tulipánt, Phys. Rev. D **94** (2016) no.7, 074019

[11] D. de Florian and M. Grazzini, Nucl. Phys. B **704** (2005) 387

[12] Z. Tulipánt, A. Kardos and G. Somogyi, Eur. Phys. J. C **77** (2017) no.11, 749

[13] P. D. Acton *et al.* [OPAL Collaboration], Z. Phys. C **59** (1993) 1.

[14] K. Abe *et al.* [SLD Collaboration], Phys. Rev. D **51** (1995) 962

[15] O. Gituliar and S. Moch, arXiv:1711.05549 [hep-ph].

[16] C. L. Basham, L. S. Brown, S. D. Ellis and S. T. Love, Phys. Rev. D **19** (1979) 2018.

[17] Y. L. Dokshitzer, G. Marchesini and B. R. Webber, JHEP **9907** (1999) 012